Nanocomposites

On the low reinforcing efficiency of carbon nanotubes in high-performance polymer fibres

--Manuscript Draft--

Manuscript Number:	
Full Title:	On the low reinforcing efficiency of carbon nanotubes in high-performance polymer fibres
Article Type:	Research Article
Keywords:	carbon nanotubes; nanocomposite; polymer fibre; polyethylene; aramid; fibre anisotropy; interface; stress transfer; micromechanics; finite element modelling
Order of Authors:	Ton Peijs
	Stergios Goutianos
Order of Authors Secondary Information:	
Additional Information:	
Question	**Response**
Author Comments:	
Funding Information:	

On the low reinforcing efficiency of carbon nanotubes in high performance polymer fibres

Stegios Goutianos[a], Ton Peijs[b,*]

[a] *Department of Manufacturing and Civil Engineering, Norwegian University of Science and Technology, Teknologivegen 22, 2815 Gjøvik, Norway*
[b] *University of Warwick, WMG, Materials Engineering Centre, CV4 7AL, Coventry, UK.*

Abstract

Driven by the exceptionally high mechanical properties of carbon nanotubes (CNTs), over the years an extensive research effort has been devoted to the reinforcement of high-performance polymer fibres with CNTs. However, to date, improvements in the strength of these fibres have been rather modest even for relatively high CNT contents. After a brief review of CNT reinforced polymer fibres, here, analytical and numerical models will be used to show that these experimental findings are to be expected based on the intrinsic mechanical properties of these polymer fibres and CNTs, their aspect ratio and interfacial characteristics. Results show that for realistic CNT contents and aspect ratios, the extraordinary strength of CNTs cannot be fully exploited in high-performance polymer fibres like Dyneema® or Kevlar®, even if these CNTs are perfectly aligned and homogeneously dispersed, due to the low intrinsic shear strength of these highly anisotropic fibres.

Keywords: Carbon nanotubes; nanocomposite; polymer fibre; polyethylene; aramid; fibre anisotropy; interface; stress transfer; micromechanics; finite element modelling

1. Introduction

Carbon nanomaterials, in particular carbon nanotubes (CNTs), have been extensively studied as a reinforcement to produce high strength, low density and highly conductive composites, owing to their exceptional mechanical and

*Corresponding author: Ton Peijs (t.peijs@warwick.ac.uk)

electrical properties [1–4]. Since their discovery [5], these materials have been considered as ideal reinforcements for a wide range of new multifunctional composites [6]. CNTs have often been considered as the next generation high performance carbon fibres due to their ultra-high strength [4, 7, 8]. While the modulus of individual CNTs (∼1 TPa) is still rather close to the modulus of some high modulus carbon fibres (600–800 GPa), their tensile strength (∼100 GPa), is some order of magnitude greater than that of the strongest carbon fibre (∼7 GPa). Despite their promise as the next generation reinforcement for polymer composites, even after several decades of exhaustive research, these high expectations have not been met yet [8, 9]. Next to the direct reinforcement of polymer matrices, several groups aimed to develop macroscopic yarns as direct replacement for carbon fibre yarns by direct spinning of aligned arrays of nanotubes [10–14]. However, unless tested at ultra-short gauge lengths, these macroscopic yarns possess mostly modest strength values, which are typically well below the strength of commercially available carbon fibre.

Also as reinforcement in polymer matrices the high expectations of CNTs have not always been met. Poor interfacial adhesion to polymer resins, their tendency to agglomerate in bundles, and their entangled nature and random organisation in polymer matrices are some of the reasons for not fully exploiting their intrinsic properties [9, 15, 16]. As with most nanocomposite studies, initial attempts to optimize properties focussed on improving the dispersion of CNTs in polymer matrices through surface modifications or the use of surfactants [17, 18]. Moreover, it was shown that effective mechanical reinforcement is only achieved with single-walled carbon nanotubes (SWCNT) rather than the more commonly used multi-walled carbon nanotubes (MWCNT) [19, 20], and only for nanotubes of high aspect ratio (>1000) [4, 8]. Even from the early introduction of CNTs it was recognised that a key aspect to the exploitation of the intrinsic properties of CNTs in polymer composites was to orient them in the matrix and to create one dimensional assemblies [21, 22]. Nanotubes can be aligned after embedding them in liquid resins by applying an electric or magnetic field [23, 24]. Alternatively, they can be oriented by flow during polymer processing [25, 26]. Particularly, fibre spinning has proven itself as a methodology that can successfully align nanotubes at relatively low loadings (<5 wt%), and a wide variety of techniques, including melt-, solution-, gel- or electrospinning [4, 15, 27–32] have all been used.

Classified by their performance, synthetic fibres can be divided into conventional textile fibres, with tensile strengths up to 1 GPa and moduli up to

∼15 GPa, and high performance fibres with tensile strengths of ∼3 GPa and moduli of ∼100 GPa. To achieve a high modulus and tensile strength, polymer molecules need to exhibit an extended chain conformation. In the case of flexible chain polymers like nylon and polyester this is (partly) achieved by solid-state drawing at elevated temperatures below the melting temperature. However, effective chain alignment requires chain disentanglement, which means that typically properties of melt-spun fibres based on flexible chain polymers are far from optimal, viz. well below their theoretical or crystal modulus [33, 34]. Until the late-1960s, nylon and polyester represented the state-of-the-art in man-made fibres, while the development of high-performance polymeric fibres started only in the early 1970s. Since then significant progress has been made in exploiting the intrinsic mechanical properties of macromolecular chains for the development of high performance fibres and two major routes were developed which differ with respect to the base material, namely, rigid versus flexible polymer chains [35].

A major breakthrough in the production of high modulus and high strength polymer fibres based on flexible chain polymers was achieved by the solution (or gel) spinning process developed at DSM in the Netherlands at the end of the 1970s [36–39]. Smith and Lemstra [36] discovered that as-spun ultra-high molecular weight polyethylene (UHMWPE) filaments from solution could be hot-stretched in the solid-state below the melting temperature to very high draw ratios. In this so-called gel-spinning process, a morphology with a very low entanglement density in the as-spun gel-like fibre is obtained, which renders them ultra-drawable. Dyneema® by DSM (Netherlands) and Spectra® by its licensee Allied Signal (now Honeywell, USA) are two commercially available high performance UHMWPE fibres. These fibres have Young's moduli that range from 80 to 150 GPa and tensile strengths of 2.5 to 4 GPa, i.e., 100 times that of bulk polyethylene [39]. In combination with their low density (<1 g/cm^3), this leads to exceptionally high specific mechanical properties (properties per unit weight), making these UHMWPE fibres of interest for a wide range of applications ranging from maritime ropes to protective gloves, bullet-proof vests, and other advanced composites applications.

The prime example of a rigid chain polymer fibre is aromatic polyamide (aramid) or poly(p-phenylene terephthalamide) (PPTA) [40]. In the late 1960s, DuPont' scientists developed para-aramid fibres that were three times as strong as nylon (∼2.5 GPa) and possessed a far higher modulus (60-120 GPa). Here, orientation with an extended chain configuration is achieved through a liquid crystalline phase spinning process. As chain extension in

these rigid rods is already built in, it is not essential to highly post-draw the as-spun filaments. Para-aramid fibres are manufactured under the trademark of Kevlar® (Du Pont, USA) and Twaron® (Teijin Aramid, Netherlands). More recent developments in the area of (semi-) rigid rod fibres includes the poly(p-phenylene-2,6-benzobisoxazole) (PBO) fibre from Toyobo (Zylon®), polyimide (PI), and aromatic polyester (Vectran®).

Over the last two decades, significant efforts were made to produce CNT reinforced polymer fibres with superior mechanical and functional properties for a wide range of polymers [27–29]. The majority of these studies involved melt- or solution spun nanotube enhanced fibres with rather modest mechanical properties based on polymers such as polypropylene (PP) [41–43], poly(ethylene therephtale) (PET) [44, 45], polyamide (PA) [46–48], polyacrylonitrile (PAN) [49, 50], poly(vinyl alcohol) (PVA) [15, 51–53], poly(lactic acid) (PLA) [54], and poly(ether ether keton) (PEEK) [55]. Although many of these studies reported increased fibre properties, only few studies achieved effective nanotube reinforcement, while none of these nanotube enhanced fibres possessed mechanical properties that are competitive with commercial high performance fibres. For the majority of these nanocomposite fibres, the effective stress carried by the CNTs, as back-calculated by a rule of mixtures relationship $\sigma_c = \sigma_f V_f + \sigma_m(1 - V_f)$, was well below 7 GPa [4], i.e. the strength of the strongest carbon fibre. In fact, for a number of nanocomposite fibres the stress carried by the CNTs did not even exceed 2-3 GPa, i.e. the strength of a baseline carbon fibre [4]. Only few nanocomposite fibres attained a reinforcing efficiency in the order of tens of GPa e.g. [41, 43, 47], albeit still well below the ultimate strength of CNTs ($\sim$100 GPa). However, a very high effective reinforcement level was achieved by Wang et al. [53] who reported a threefold increase in strength, from 400 to 1200 MPa, with the addition of 1 wt% SWCNT in oriented PVA. Evaluating the data using the rule of mixtures resulted here in an effective nanotube stress contribution of 88 GPa, viz. approaching the ultimate tensile strength of SWCNTs.

As mentioned earlier, while some of above studies reported nanotube reinforcement, the majority of these fibres possessed overall mechanical properties that were well below those of commercial high performance polymer fibres with typical tensile strengths in the order of 2-3 GPa. However, given their ultra-high tensile strength potential, the prospect of a substantial increase in tensile strength of high performance fibres through the introduction of CNTs is still very intriguing [27, 56–60]. Especially their introduction in fibres based on rigid rod polymers seemed appropriate since CNTs themselves

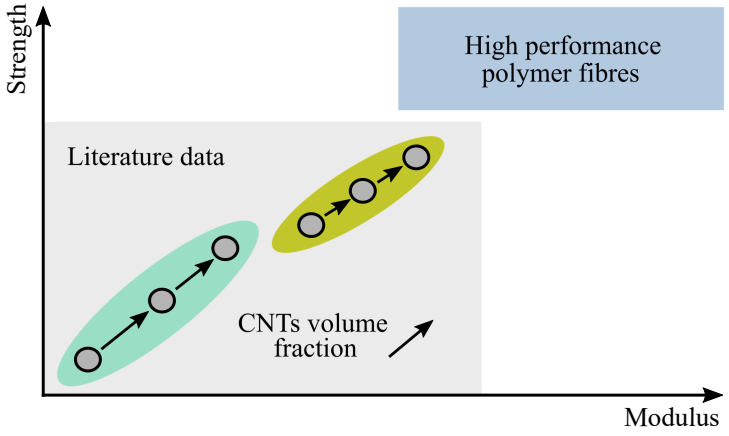

Figure 1: Typical reinforcing effect of CNTs on the modulus and strength of polymer fibres with low or medium properties as compared to commercial high performance fibres.

can exhibit liquid-crystalline behaviour [61, 62]. Current achievements in reinforcing polymer fibres with CNTs are shown schematically in Fig. 1: efficient reinforcment is typically reported for polymer fibres with relatively modest strength and stiffness, whereas little data exists that demonstrates major improvements in strength and stiffness of high performance polymer fibres. Kumar et al. [56] showed that the strength of PBO fibres increased by 60% with a SWCNT volume fraction of 10%. However, although interesting and significant, even at a 10 times higher CNT content, this increase was still considerably less pronounced as the earlier mentioned PVA fibre [53] with an effective nanotube stress contribution of 19 GPa for PBO as compared to 88 GPa for PVA [4, 27]. Moreover, it should also be noted that the Young's modulus of the PBO fibres used by Kumar et al. [63] possessed only half the modulus of commercial PBO fibres (270 GPa), meaning that the effective reinforcement effect in such higher modulus fibres would probably be less. Similar results were reported by Ruan et al. [57, 58] for MWCNT reinforced UHMWPE fibres. By adding 5 wt% MWCNTs, the strength of UHMWPE fibres, with a Young's modulus of around 120 GPa, increased by approximately 20%. Although this study also reported a significant increase in strength (4.2 GPa as compared to 3.5 GPa for neat fibre), the question remains in this and many other related studies if this increase in strength is the direct result of reinforcement by the CNTs or merely the result of a more favourable morphology for subsequent ultra-drawing. In other words, did the improvements in fibre properties come directly from the nanofiller

or indirectly from a modification of the polymer matrix by the nanofiller, leading to higher draw ratios and improved mechanical properties [53, 64]? Moreover, since the dimensions of CNTs are comparable to the unit cell of polyethylene, their presence may affect the packing density of these chains and as a result ultimate mechanical properties [65]. Nanotube reinforcement in aramid fibres has also been investigated [44, 66]. Deng at al. [66] prepared PPTA/SWNT nanocomposite fibres by a dry-jet wet spinning process and different draw ratios. As the presence of nanotubes affected the polymer chain orientation in the nanocomposite fibres, particularly at higher draw ratios, mechanical properties were mostly reduced. Although efficient stress transfer was observed through in-situ Raman spectroscopy, a breakdown of the interface above 0.35% strain (∼35 GPa) occurred [66], making these nanotubes basically ineffective at higher strains and stresses.

Hence, given the limited success of CNTs to reinforce high performance polymer fibres, the question arises if CNTs - even in theory - can effectively reinforce such fibres e.g. significantly improve their modulus and strength even further (see Fig. 1). To answer this, here, both analytical and finite element models will be employed to study the reinforcing potential of CNTs in high performance polymer fibres as a function of fibre properties, CNT content and interface conditions, while assuming that the CNTs are perfectly aligned and homogeneously dispersed within the polymer fibre.

2. Analytical Modelling

Among an extensive number of analytical micromechanical composite models available, the models of Hale and Kelly [67] and Sørensen [68] will be used in the present work. The first model is intended to examine the maximum possible reinforcing effect of CNTs in oriented polymer fibres e.g. infinitely long and well aligned CNTs, which are also perfectly bonded to the polymer matrix, i.e. polymer fibre. The second model, which includes interfacial debonding, frictional sliding and residual stresses, will be used to investigate the efficiency of CNTs of finite length under more realistic conditions. Both analytical model allow us to study the effect of a wide range of material parameters on the strength improvement of high performance polymer fibres by CNTs. For completeness, the two analytical models are briefly discussed below.

2.1. Infinitely long aligned CNTs in a polymer fibre without debonding

For infinitely long, perfectly aligned CNTs of equal strength, the minimum CNT volume fracture, V_{min}, which increases the strength of a polymer fibre, σ_f^u, depends on the failure strain of the CNTs compared to the failure strain of the polymer fibre [67]. When the CNTs are brittle relative to the polymer fibre ($\epsilon_{CNT}^u < \epsilon_f^u$), then V_{min}, is:

$$V_{min} = \frac{\sigma_f^u - \sigma_f'}{\sigma_{CNT}^u + (\sigma_f^u - \sigma_f')}, \quad for \quad \epsilon_{CNT}^u \leq \epsilon_f^u \tag{1}$$

where σ_f^u is the strength of the polymer fibre, σ_{CNT}^u the CNTs strength and σ_f' is the stress in the polymer fibre required to induce a strain equal to the failure strain of the CNTs. SWCNTs, with strengths of around 100 GPa, in most cases will have a higher failure strain than a typical high performance polymer fibre, $\epsilon_{CNT}^u > \epsilon_f^u$, [69]. Hence, the minimum CNTs volume fracture, V_{min}, is [67]:

$$V_{min} = \frac{\sigma_f^u}{\sigma_{CNT}^u - (\sigma_{CNT}' - \sigma_f^u)}, \quad for \quad \epsilon_{CNT}^u > \epsilon_f^u \tag{2}$$

where σ_{CNT}' is equal to $E_{CNT}\epsilon_f^u$ and E_{CNT} is the effective Young's modulus of the CNTs. The underlying assumption, that the CNTs and polymer fibre are linear elastic, is reasonable for highly oriented high performance polymer fibres within the context of the present work.

Eqs. 1 and 2 should be considered as the lower limit of V_{min} since, apart from the conditions mentioned above, it is also assumed that the CNTs are perfectly bonded to the polymer fibre.

2.2. Infinitely long aligned CNTs in a polymer fibre with debonding

A more realistic model, compared to the previous model, should consider debonding of the infinitely long CNTs from the polymer fibre as shown in Fig. 2. At a certain applied stress, a CNT will debond from the polymer fibre at the CNT ends. This stress, denoted as debonding initiation stress, σ_c^i, is given by [68]:

$$\frac{\sigma_c^i}{E_c} = \frac{(1 - V_{CNT})E_f}{E_c}\Delta\epsilon^T + 2\sqrt{\frac{(1 - V_{CNT})E_f}{E_c}\left(\frac{\mathcal{G}_{c,t}^i}{E_{CNT}r_{CNT}}\right)} \tag{3}$$

where E_c and E_f are the moduli of the reinforced and unreinforced polymer fibre. The CNTs, with radius r_{CNT}, have a volume fraction V_{CNT}. The misfit strain, $\Delta\epsilon^T$, is due to the difference in thermal expansion of the CNTs and the polymer fibre. The interface properties expressed by the mode II (shear) fracture energy, $\mathcal{G}^i_{c,t}$, affects also the debonding initiation stress.

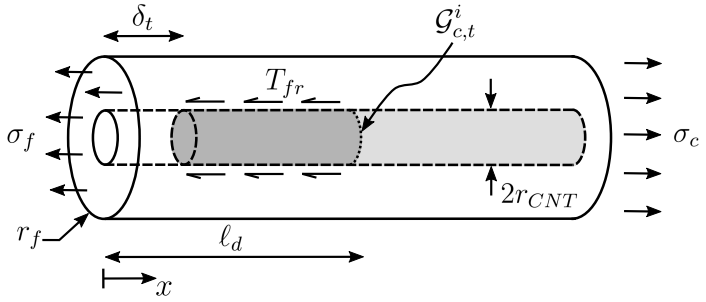

Figure 2: A single infinitely long CNT embedded in a polymer fibre cylinder. Upon loading, the CNT debonds at applied stress σ^i_c (debonding initiation stress). After debonding initiation, the CNT slides in the debonded zone. The frictional stress is denoted as T_{fr}.

If there is no friction, then Eq. 3 gives the stress level at which the debond crack will propagate along the entire CNT/polymer fibre interface, thus giving a lower bound strength. The difference in strain and surface roughness may induce an interface frictional stress, T_{fr}. This frictional stress results in an increase in applied stress, σ_c, as the debond length, ℓ_d, increases [68]:

$$\frac{\sigma_c}{E_c} = \frac{\sigma^i_c}{E_c} + 2\left(\frac{T_{fr}}{E_{CNT}}\right)\left(\frac{\ell_d}{r_{CNT}}\right) \tag{4}$$

It is clear that the applied stress, σ_c, is linearly related to the debond length and higher than the debonding initiation stress σ^i_c. The debond length is:

$$\begin{aligned}\frac{\ell_d}{r_{CNT}} = \frac{E_{CNT}}{2T_{fr}}\left(\frac{\sigma_c}{E_c} - \frac{(1-V_{CNT})E_f}{E_c}\Delta\epsilon^T\right) \\ -\frac{E_{CNT}}{T_{fr}}\sqrt{\frac{(1-V_{CNT})E_f}{E_c}\left(\frac{\mathcal{G}^i_c}{E_{CNT}r_{CNT}}\right)}\end{aligned} \tag{5}$$

It should be noted that the axisymmetric micromechanical model of

Sørensen [68] is originally developed to study debonding initiation and growth from a fibre break location for an infinitely long fibre.

2.3. Interface cohesive law

The mode II (shear) interface fracture energy, $\mathcal{G}^i_{c,t}$, in Eq. 3 can be regarded as a property of the CNT/fibre interface cohesive law e.g. a relation between the normal and shear tractions at the interface and the corresponding opening and tangential displacements [70, 71]. The traction in the cohesive zone may originate from Van der Waals forces, chemical bonding or interface friction or a combination of these [1, 72, 73]. Fig. 3 shows such a cohesive law, the mode II (shear) component, which in its simplest form shows a linear softening behaviour. The mode II (shear) traction decreases from its peak value, $\hat{T}_t$, to zero when the interface tangential crack opening reaches the critical mode II tangential (or sliding) opening δ^f_t. The area under the traction-separation curve equals the mode II (shear) interface fracture energy, $\mathcal{G}^i_{c,t}$. If friction exists at the interface, then the mode II traction decreases to the frictional stress, T_{fr}, and then remains constant as the tangential opening further increases. In Fig. 3 it is assumed that the mode II traction becomes equal to T_{fr} when $\delta_t = \delta^f_t$. The area under the traction-separation curves for crack openings larger than δ^f_t is equal to the dissipated energy due to friction.

It should be noted that the cohesive law of Fig. 3 is a phenomenological cohesive law commonly used in solid mechanics for modelling crack initiation and propagation along interfaces or material planes [74, 75]. The cohesive law concept (Fig. 3) allows in the present work to relate the analytical predictions using the model of Section 2.2 to the numerical predictions using the finite element models introduced in the next section.

3. Finite element modelling

The finite element model (FE) used here is based on the CNT distribution shown in Fig. 4a, where it can be seen that the CNTs have a finite length, $2\ell_{CNT}$, and there is a partial overlap between neighbouring CNTs. The distance between lines passing through the CNTs centers is ℓ_c.

Fig. 4b shows a cross-section normal to the CNTs (only half of the CNTs are cut), assuming a square array of CNTs of a rectangular cross-section and with length r_{CNT}. A more natural way would be to assume circular CNTs with a radius r_{CNT} surrounded by a fibre of radius r_c (Fig. 4b). This would

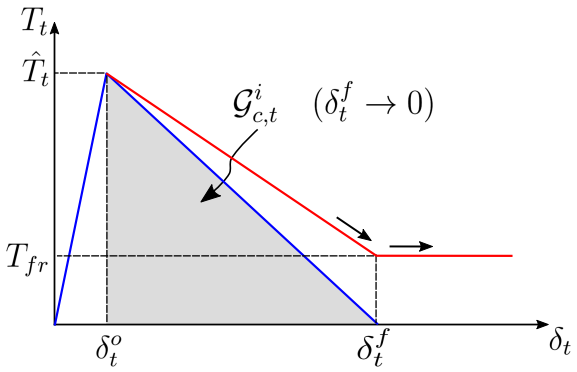

Figure 3: Schematic illustration of the mode II interface cohesive law with linear softening. When the interface friction is zero the shear traction, T_t, decreases to zero when $\delta_t = \delta^f_t$ and the area under the traction-separation curve is the mode II interface fracture energy, $\mathcal{G}^i_{c,t}$. When interface friction is implemented, the shear traction is reduced to the frictional stress, T_{fr}, when $\delta_t = \delta^f_t$ and then it remains constant. For the mode I (normal) interface cohesive law, T_n decreases to zero when the normal crack opening equals the normal critical opening δ^f_n.

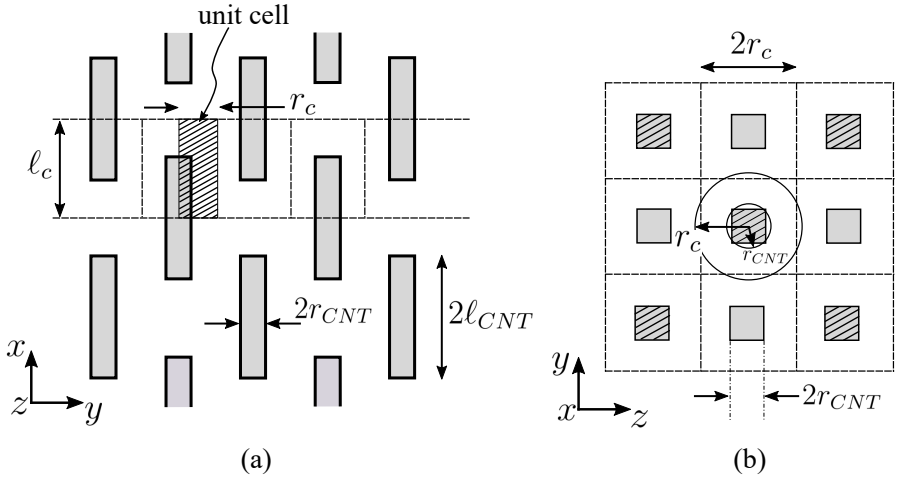

Figure 4: Periodic array of aligned CNT of finite length: a) Cross-section parallel to CNTs and b) cross-section normal to CNTs.

allow to approximate the 3D problem of Fig. 4 by an axisymmetric model indicated by the hatched region and shown in more detail in Fig. 5 [76]. A critical parameter for achieving a high reinforcing efficiency of CNTs is a high interface shear peak traction, $\hat{T}_t$, defined in the previous section. A drawback

of the analytical model of Section 2.2 is that failure of the polymer fibre itself is not considered. By assuming a rectangular cross-section for the CNTs, the composite damage model [77, 78], available in the Abaqus commercial finite element code for plane stress problems, can be applied to allow failure of the polymer fibre. Numerical tests, without polymer fibre damage and failure, have shown that the plane stress models yield very similar results to the corresponding axisymmetric models for a wide range of parameters examined. Thus, the assumption of plane stress conditions is considered reasonable and will be used in the present work.

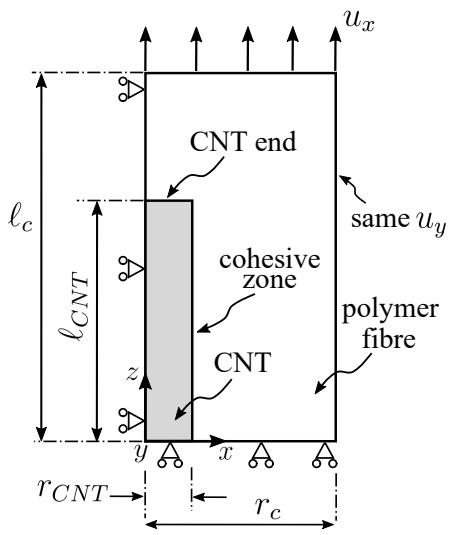

Figure 5: 2D finite element unit cell model: materials, geometry and boundary conditions and symmetry planes.

Fig. 5 shows the geometry and boundary conditions of the unit cell analysed. Due to symmetry, only a quarter of the geometry is modelled. The radius of the CNTs, r_{CNT}, is equal to 1.5 nm and the length, ℓ_{CNT}, is equal to 3 mm, i.e. an aspect ratio is assumed of 2000. The total length of the model is ℓ_c and therefore $\ell_c - \ell_{CNT} = (3/8)\ell_{CNT}$ (see Fig. 4a). It should be noted that the overlap length of the CNTs has a negligible effect on the results. The width of the model, r_c, is varied depending on the CNT volume fraction. The CNT end is assumed to be fully debonded from the polymer matrix or fibre, an assumption which has also a negligible effect on the results. The CNT/polymer fibre interface is modelled with cohesive elements. The constitutive law (cohesive law) is given in Fig. 3. The cohesive elements

have a length of 0.2 nm and a finite thickness equal to 0.05 nm. With this cohesive element length, the number of cohesive elements within the fracture process zone, $\delta_t^o \rightarrow \delta_t^f$, is in the order of 300, much larger than the minimum required number of cohesive elements which is 4 to 7 [79] in order to get accurate results. The Abaqus explicit solver is used to solve the problem of Fig. 5 under quasi-static conditions using mass-scaling. An explicit solver is preferred to avoid convergence difficulties, which are commonly observed when modelling crack growth with implicit finite element methods [80, 81].

4. Materials properties

The properties of CNTs have been investigated experimentally, numerically and theoretically. Krishnan et al. [82] have experimentally estimated the Young's modulus of SWCNTs to be about 1.25 TPa. A similar value, 1.28 TPa, was experimentally obtained by Wong et *al.* [83]. Jin et al. [84], using molecular dynamics, calculated the effective Young's modulus between 1.23 to 1.35 TPa. The Young's modulus, based on finite element analysis, was calculated between 1.1 and 1.32 TPa [85] and equal to 0.7 or 1 TPa based on micromechaniccal analysis [86, 87]. In the present work, for the analytical models, the CNTs are assumed isotropic linear elastic with E_{CNT} =1 TPa. An exact value for E_{CNT} it is not crucial for the current work. In the finite element analysis, the CNTs are modelled as anisotropic linear elastic solids. The elastic properties are given in Table 1, which are based on theoretical and numerical analyses [84, 85, 88]. The polymer fibres are modelled as isotropic linear solids in the analytical models. In specific cases where an UHMWPE fibre is assumed, the fibre's Young's modulus, E_f, is set equal to 80 GPa [39, 89]. The anisotropic UHMWPE fibre elastic properties as used for the finite element analysis, are listed in Table 1 and they are based on the experimental work of Peijs et al. [89].

Table 1: Elastic properties of CNTs and UHMWPE fibre.

	E_{11} (GPa)	E_{22} (GPa)	E_{33} (GPa)	ν_{12} (-)	ν_{13} (-)	ν_{23} (-)	G_{12} (GPa)	G_{13} (GPa)	G_{23} (GPa)
CNT	1000	60	60	0.25	0.05	0.05	500	25	25
UHMWPE	80	2	2	0.3	0.01	0.01	0.8	0.3	0.3

$1 \rightarrow x$, $2 \rightarrow y$, $3 \rightarrow z$. $E_{11} = E_{CNT}$ for CNTs and $E_{11} = E_f$ for UHMWPE fibre.

Table 2: Strength properties of UHMWPE fibre [89].

$\sigma_f^u = \sigma_{11}^u$ (MPa)	σ_{22}^u (MPa)	σ_{33}^u (MPa)	σ_{12}^u (MPa)	σ_{13}^u (MPa)	σ_{23}^u (MPa)
3600	14	14	10	10	10

Predictions of the intrinsic tensile strength of SWCNTs are in the order of 100 GPa and higher: 117 GPa [90], 110 GPa [91], and 93 GPa [69]. A wide range of experimental strength values were reported: 150 GPa [92], 25 to 75 GPa [93], and 13 to 52 GPa [94]. In the present work, the tensile strength of CNTs is taken as equal to 140 GPa, i.e. close to the theoretical and numerical predictions. In the finite element analyses, it is assumed that the CNTs do not fail. The strength of the UHMWPE fibre is taken as equal to 3.6 GPa for the analytical models, whereas the experimentally determined anisotropic strength values used are based on the values given in Table 2 [37, 39, 89]. In the finite element analyses (FEA), the transverse tensile strength, transverse compressive strength and axial compressive strength are equal to 100 MPa to promote failure by shear. The polymer shear strength values are between 20 to 100 MPa e.g. lower and higher than the peak traction (interfacial shear strength), $\hat{T}_t$, which is used in the cohesive law. It should be noted that even the lower shear strength value is higher than the intrinsic shear strength values of of UHMWPE fibre listed in Table 2. However, the parameter that governs the fracture of the CNT reinforced fibres is the ratio of the mode II (shear) peak traction over the shear strength of the polymer fibre.

The interfacial shear strength of the CNT/polymer interface has been extensively investigated both experimentally and theoretically. Experimental data reported includes for example shear strength values that vary as widely as 14.4 and 366 MPa for epoxy resin [95, 96], and 160 MPa for functionalized CNTs in polyvinyl alcohol [97]. A review on experimentally obtained interfacial shear strength values for different polymers [98] shows that the interfacial shear strength typically varies between 30 and 100 MPa. On the other hand, only a small number of studies theoretically predicts the CNT/polymer interface cohesive law [72, 73]. An (unrealistic) peak traction, $\hat{T}_t$, was predicted of approximately 450 MPa with a critical opening, δ_t^f, in the order of 3 nm. In the present work, a large range of $\hat{T}_t$ was examined, whereas in the finite element analyses $\hat{T}_t$ is equal to 25 MPa, which, according to the authors opinion, is of a more realistic order of magnitude. The critical crack opening, δ_t^f, is varied from 0.1 to 5 nm.

Thermal effects were ignored e.g. $\Delta\epsilon^T = 0$. The main effect $\Delta\epsilon^T$ is friction along the CNT/polymer interface, which is modelled by prescribing a constant frictional stress in the analytical model of Section 2.2 and by using a mode II (shear) cohesive law with constant traction for shear openings larger than δ_t^f (see Fig. 3). In other words, friction is directly included in the cohesive law instead of prescribing frictional contact once $\delta_t > \delta_t^f$.

5. Results and Discussion

5.1. Aligned CNTs of infinite length in a polymer fibre with perfect bonding

Fig. 6 shows an example of the strength of an UHMWPE fibre reinforced with CNTs as a function of the CNT volume fraction. Using Eq. 2, it can be seen that the minimum CNT volume fraction, V_{CNT}, above which a significant reinforcement effect of the UHMWPE fibre is obtained is approximately 3.6%. Perfect dispersion at this volume fraction is already hard to achieve in practice [99], while in order to have a significant reinforcement effect a much higher SWCNT content would be required. For example, only at at V_{CNT} equal to 7.5%, the CNT reinforced UHMWPE fibre would have a strength of ∼10 GPa, i.e. three times that of the unreinforced polyethylene fibre, and higher than the highest strength commercial carbon fibre.

Using Eqs. 1 and 2, results such as the one presented in Fig. 6 can be summarised in the contour plot of Fig. 7 where V_{min} is plotted as a function of neat polymer fibre Young's modulus, E_f, and tensile strength, σ_f^u. Fig. 7 focuses on highly oriented high modulus polymer fibres as can be seen by the x-axis scale. In this graph, the Young's modulus and strength of known commercial high performance polymer fibres like Kevlar®, Dyneema®, Spectra® and Zylon® are superimposed. It can be seen that for higher performance fibres, the minimun CNT volume fraction, V_{min}, for effective reinforcement increases to levels that cannot be easily achieved while maintaining perfect dispersion of individual nanotubes for practical reasons. For example, if Zylon® fibres were to be reinforced, a CNT volume fraction greater than 5% would be required just to reach V_{min}. Of all commercial high performance fibres, only for the lower performance Spectra 900 or Dyneema SK60 fibre, V_{min} is below 2.5%. If a non-commercial PVA fibre with a Young's modulus of 15 GPa is considered [53] (note that the Young's modulus of commercial high performance PVA fibre can be as high as 40 or 50 GPa), V_{min} is approximately equal to 0.35%, i.e. a filler content where homogeneous dispersion of individual CNTs in more readily achievable. If the CNT volume fraction is

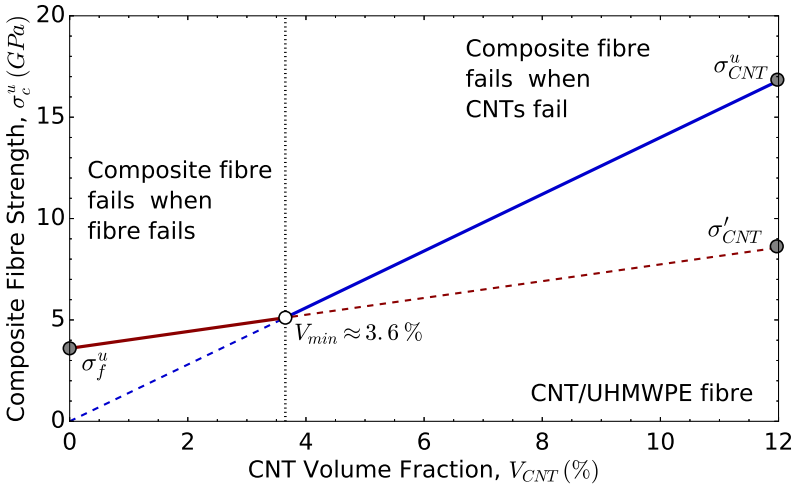

Figure 6: Minimum CNT volume fraction, V_{min}, for effective reinforcement of an UHMWPE fibre with a strength of 3.6 GPa (strain at break of CNT > strain at break polymer fibre).

increased to 0.85%, Eq. 2 predicts that the strength of the CNT reinforced PVA fibre will increase by a factor of three, a value close to the experimental results of Wang et al. [53] where the corresponding CNT volume fraction for a strength increase by a factor of 3 was 1.0 wt% (∼0.8 vol%). Thus, Eq. 2 predicts relatively accurate the reinforcing effect of CNTs at least for polymer fibres of moderate mechanical properties.

A graph like Fig. 6 is well known and well understood for traditional unidirectional composites based on glass or carbon fibres [100]. However, since the minimum reinforcement (fibre) volume fraction, V_{min}, for traditional composites is typically only a few percent, i.e. several times lower than practical fibre volume fractions (50-60%), the relevance of V_{min} is generally not recognised. In case of nanocomposites, however, with filler loadings typically around a few percent, Fig. 6 becomes highly relevant.

5.2. Aligned CNTs of finite lenght in a polymer fibre with debonding

Although the CNTs considered in the model have a very high aspect ratio, $AR = 2\ell_{CNT}/(2r_{CNT})$, they are not infinitely long as assumed in Section 5.1. Interfacial debonding can initiate from the CNT ends and propagate along the interface, thus reducing the reinforcing efficiency of the CNTs.

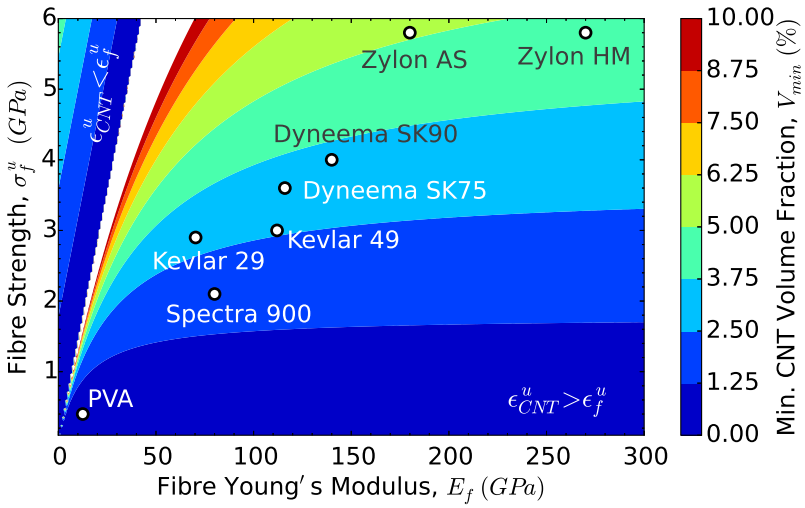

Figure 7: Minimum CNT volume fraction for effective polymer fibre reinforcement as a function of the fibre properties E_f and σ^u_f. Data for the high performance polymer fibres are taken from [39], and for the non-commercial PVA fibre from [15].

Fig. 8 shows the debonding initiation stress, using Eq. 3, as a function of the polymer fibre Young's modulus, E_f, and the interface mode II (shear) peak traction, $\hat{T}_t$, for V_{CNT} equal to 6%, which is higher than V_{min} for all cases.

From $\hat{T}_t$ and assuming a critical tangential opening, δ_{tf}, equal to 5.0 nm, the mode II (shear) fracture energy, $\mathcal{G}^i_{c,t}$, can be calculated (see Fig. 3) and used in Eq. 3. A value of 5.0 nm is probably rather large [73] and therefore Fig. 8 gives a non-conservative debonding initiation stress, σ^i_c. The characteristic properties, Young's modulus and strength, of four commercial high performance polymer fibres are also plotted. If it is assumed that there are no frictional stresses (see Section 2.2), then the strength of the reinforced polymer fibres, σ^u_c, is equal to the debonding initiation stress. Then, if a Spectra 900 fibre is considered, it can be seen that the interfacial shear peak traction should be higher than 60 MPa in order to have a debonding initiation stress that exceeds the strength of the fibre itself and thus results in a minimum positive reinforcement effect of the polymer fibre. For the Dyneema SK90 fibres, the corresponding required interfacial shear peak traction is close to 100 MPa, for the Zylon AS fibre more than 100 MPa, whereas for the Zylon HM it is approximately equal to 165 MPa. Hence, for most

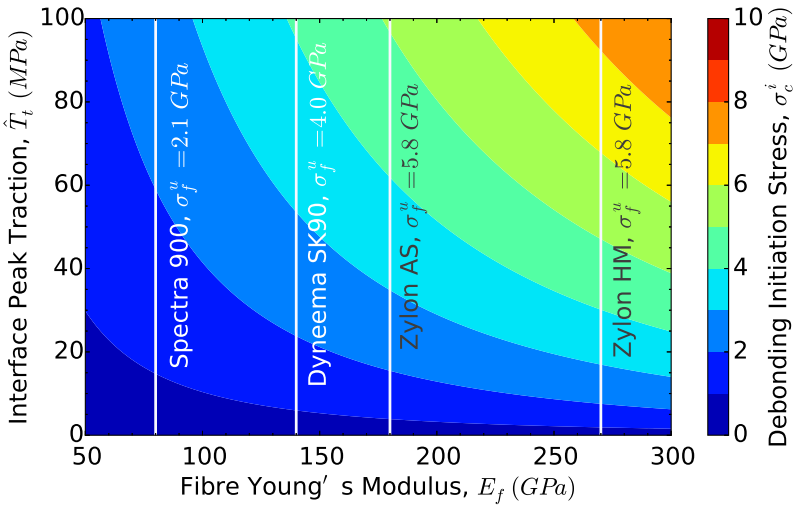

Figure 8: Stress for debonding initiation, σ_c^i, as a function of the polymer fibre Young's modulus, E_f, and the interface peak traction, $\hat{T}_t$. For T_{fr} =0, $\sigma_c^u = \sigma_c^i$. Interface: δ_{tf} =5.0 nm. The CNT volume fraction is 6.0% $> V_{min}$.

high performance polymer fibres, a high interface peak traction is required to delay initiation of debonding and to achieve a positive reinforcing effect of CNTs on the strength of these high performance polymer fibres. In many cases the calculated required interfacial shear peak traction exceed however the intrinsic shear strength of these highly anisotropic polymer fibres. Here, the favourable characteristics in the fibre (chain) direction in terms of stiffness and strength are not matched at in off-axis loadings. Fibre anisotropy exists in all high-performance organic fibres. In aramid fibres the PPTA molecules are covalently bonded in one dimension (1D) [40]. In comparison with UHMWPE fibres we could therefore refer to them as (1D+) structures due to the stronger hydrogen bonds between the polymer chains in comparison with the weak Van der Waals interactions in polyethylene. As a result of this, the transverse and shear properties of these fibres can be up to two orders of magnitude lower than their uniaxial tensile properties. Realistic values for the intrinsic shear strength lie somewhere between 10 and 30 MPa for UHMWPE fibres and 60 and 80 MPa for aramid [39, 89, 101], with PBO somewhere in between. Hence, irrespective of the level of interfacial adhesion the stress transfer is often limited by the intrinsic shear strength of the polymer fibre rather than that of the interface. In the next section, FEA results

will further examine if such high interface peak tractions can lead to CNT reinforced polymer fibres with significantly improved strength properties.

Next in Fig. 9 the combined effect of CNT volume fraction and interface shear peak traction on the debonding initiation stress is examined. The fibre properties are identical to the UHMWPE fibre of Fig. 6 e.g. E_f =80 GPa and σ_f^u =3.6 GPa. For this fibre, under the assumptions of the model of Section 2.1, V_{min} =3.6%. From Fig. 9a, with a large δ_t^f and thus large $\mathcal{G}_{c,t}^i$, it can be see that in case of interfacial debonding the volume fraction of CNTs has to be increased close to 10%, together with an interface shear peak traction of approximately 200 MPa, in order to have a minimum positive reinforcement effect. When decreasing the required interfacial peak traction, for example by a factor of two, the CNT volume fraction has to be larger than 30-40% in order to create a CNT reinforced fibre with a higher strength than the unreinforced fibre itself. Fig. 9a shows that a high debonding initiation stress, i.e. greater than the tensile strength of the unreinforced fibre, can only be achieved by a combined high CNT volume fraction ($>$ 30 vol%) and high interfacial shear peak traction ($>$ 150 MPa), which is difficult if not impossible to achieve. For a more realistic interfacial shear peak traction in the order of 25 MPa, the debonding initiation stress is approximately 1.2 GPa for CNT volume fractions as high as 50%. Even for such a high CNT content this value is only one third of the unreinforced fibre strength e.g. in this case the CNTs actually reduce the fibre strength significantly. When the critical interfacial shear crack opening is reduced from 5.0 nm to 0.5 nm (Fig. 9b), then even for interface peak tractions up to 200 MPa and CNT volume fractions up to 50%, the strength of the CNT reinforced UHMWPE fibre is well below that of the neat polymer fibre. It is clear that conditions that can lead to increased fibre strength are difficult if not impossible to achieve in practical fibre systems.

The predictions of Figs. 8 and 9 are more realistic than the predictions of Fig. 7. However, they are still conservative as it is assumed that once debonding initiates at the CNT end, it will propagate at a constant stress along the entire nanofibre interface. The presence of interfacial frictional stresses will require a higher applied stress to further increase the debond length, ℓ_d, as Eq. 4 states e.g. a linear relationship between the applied stress and debonding length, which is given by Eq. 5. The effect of the interfacial friction is shown in Fig. 10 where the strength of a nanoreinforced UHMWPE fibre is plotted for different CNT volume fractions. Here, the

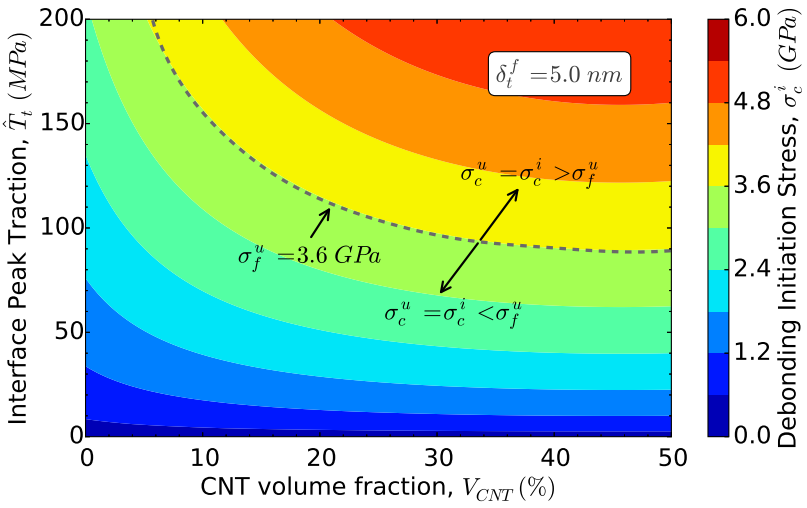

(a)

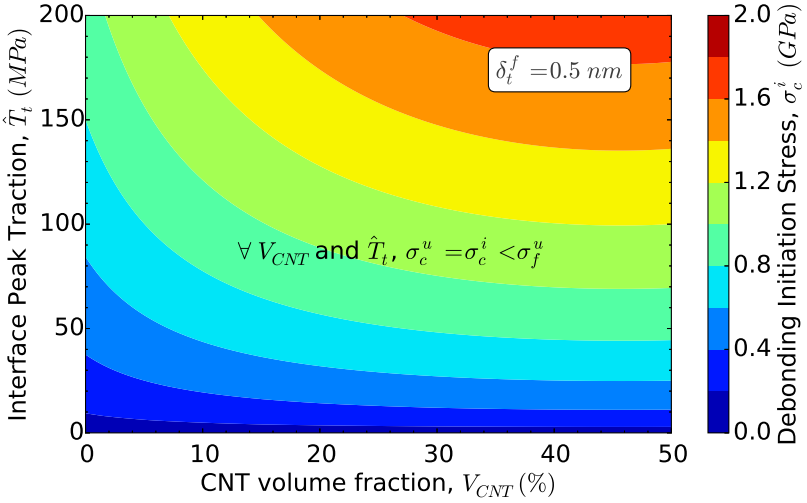

(b)

Figure 9: Stress for debonding initiation, σ_c^i, as a function of the CNTs volume fraction, V_{CNT}, and the interface peak traction, $\hat{T}_t$ for δ_t^f =5.0 nm and 0.5 nm, respectively. For $T_{t,fr}$ =0, $\sigma_c^u = \sigma_c^i$.

interface friction is equal to 1 MPa and the polymer fibre properties are

the same as in Figs. 7 and 9. As discussed above (see Fig. 9), debonding initiates at a stress significantly lower than the fibre strength. In Fig. 10 the debonding initiation stress is when the debond length is greater than zero. It can be seen that for all CNT loadings, the applied stress has to be increased in order to propagate the interface crack. If the case of V_{CNT} =10% is considered, then it can be see that debonding starts when σ_c ∼1.45 GPa. If the CNTs have an aspect ratio, AR, equal to 1000 and the debond crack initiates and propagates from both CNT ends, then the CNTs will be fully debonded when σ_c ∼1.6 GPa, which is still nearly half the original fibre strength (3.6 GPa). Even for an aspect ratio of 5000, the CNT "reinforced" fibre has a predicted strength below that of the unreinforced fibre (2.28 GPa). For an even higher aspect ratio, of around 10000, the nanocomposite fibre has a strength of approximately 3.15 GPa, which is still slightly lower than the neat fibre at 3.6 GPa. Only when V_{CNT} is 15% and AR is equal to 10000, the reinforced nanocomposite fibre has a ∼4% higher strength than the neat UHMWPE fibre. This highlights the importance of aspect ratio and is in agreement with recent analytical studies, based on simple shear-lag models, for graphene reinforced nanocomposites, where properties are also limited by the filler aspect ratio [102]. For low V_{CNT} (<1%), the reinforced nanocomposite fibre strength is approximately half that of a neat UHMWPE fibre even for high aspect ratios CNTs.

As shown in Fig. 9, for a constant mode II peak traction, an increase of the critical interfacial crack opening, δ_t^f, increases the mode II (shear) fracture energy and thus the stress for debonding initiation increases. The same can be seen in Fig. 11 where interfacial crack growth is taken into account. The critical crack opening has a significant effect on the tensile strength of the CNT reinforced polymer fibre. For example, for AR equal to 10000, there is a 25% reduction in strength by decreasing δ_t^f from 5 to hl1 nm.

In Fig. 12 the interface frictional stress, T_{fr}, is varied for V_{CNT} equal to 10%. For this CNT volume fraction and T_{fr} =1 MPa, it was shown in Fig. 10 that the strength of the CNT reinforced nanocomposite fibre is lower than the strength of the polymer fibre itself even for AR =10000. By increasing the frictional stress to 2 MPa, the strength of the CNT reinforced fibre increases by 35%. A further increase of T_{fr} =5.0 MPa, results in a three times higher strength, whereas for large values of T_{fr} equal to 15 MPa, the reinforced fibre has a strength of more than 7 times the strength of the unreinforced fibre. For low aspect ratios CNTs, AR =1000, even frictional stresses as high as

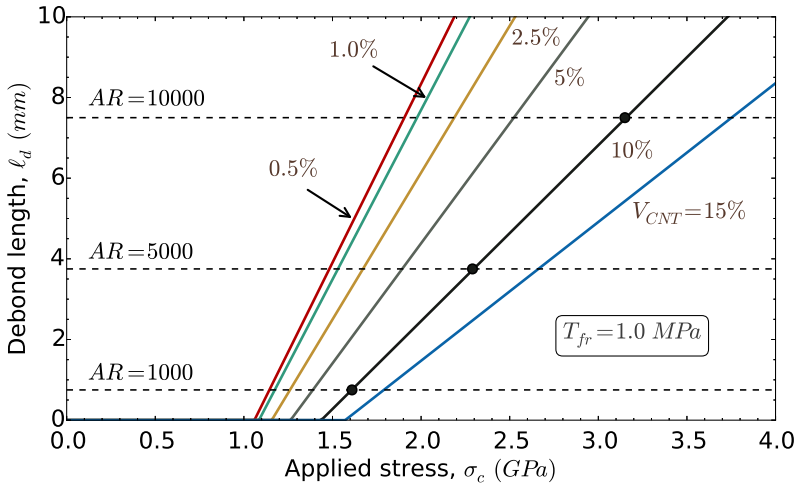

Figure 10: Debond length, ℓ_d, as a function of the applied composite stress, σ_c, for different CNT volume fractions and interface friction equal to 1 MPa. The dashed lines represent when the CNTs are fully debonded for CNTs of three different aspect ratios, AR, and considering that debonding starts from both CNT ends. Interface: $\hat{T}_t$ =25 MPa, δ_t^f =5.0 nm.

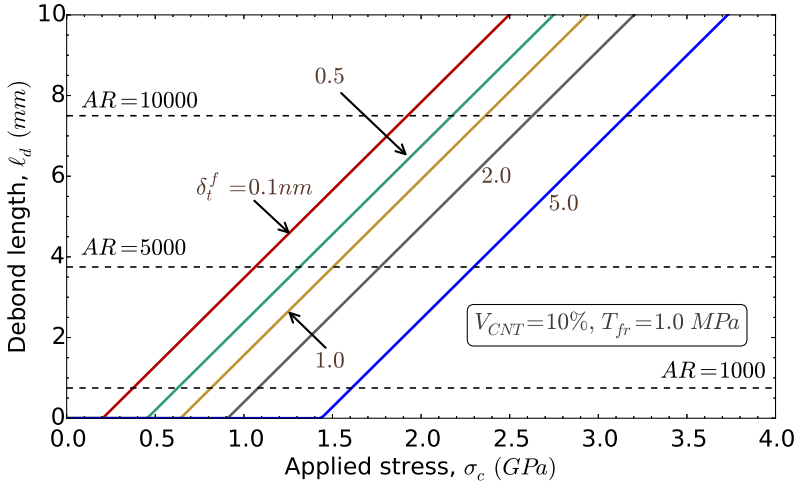

Figure 11: Debond length, ℓ_d, as a function of the applied composite stress, σ_c, for different critical interfacial shear crack openings δ_t^f. Interface: $\hat{T}_t$ =25 MPa, T_{fr} =1.0 MPa.

10 MPa do not improve the fibre strength. Even for T_{fr} =15.0 MPa, the improvement in strength is only approximately 10%. The results of Fig. 12 can be compared with the results of Fig. 9 and it can be concluded that only in the case of large (unrealistic) interfacial frictional stresses, significant improvements in fibre strength can be achieved without the need of very high and unrealistic interfacial shear peak tractions due to the high CNT aspect ratio.

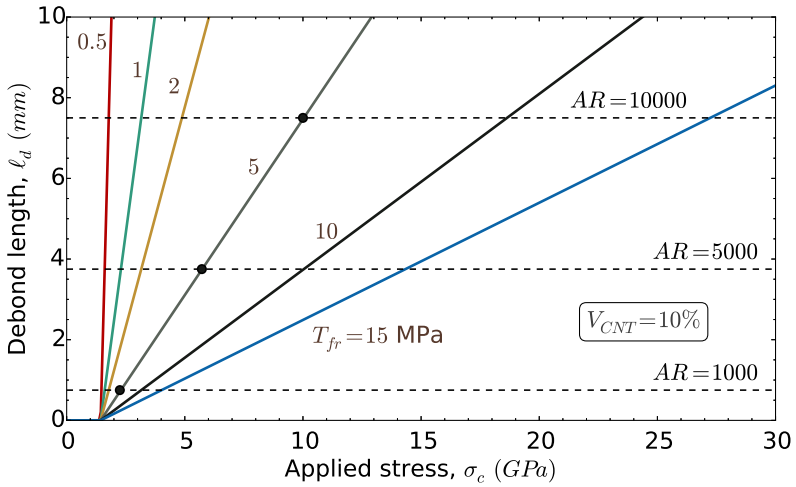

Figure 12: Debond length, ℓ_d, as a function of the applied composite stress, σ_c, for different interface frictional stresses and a CNT volume fraction equal to 10%. The dashed lines represent when the CNTs are fully debonded for CNTs with three different aspect ratios, AR, and considering that debonding starts from both CNTs ends. Interface: $\hat{T}_t$ =25 MPa, δ_t^f =5.0 nm.

Based on the results of this section, it can be concluded that in theory CNTs can reinforce high performance polymer fibres but only under certain conditions or more precisely a combination of them: high CNT volume fraction (e.g. >10 %), of very high aspect ratio (>10000) and relatively high interface frictional stresses (>15 MPa). However, in practice, such high values for V_{CNT} and interfacial friction are not always easily achievable. For example, it is well established that nanofiller dispersion becomes more difficult at higher filler loading, leading to agglomeration and ineffective reinforcement [43]. Even if homogeneous dispersions of individual CNTs at high concentrations and high interfacial adhesion can be achieved, effective stress transfer

may still be limited by the intrinsically low shear strength of high performance polymer fibres. This will trigger other fibre dominated failure modes, which may result in a lower fibre strength. These issues will be examined in more detail in the next section using finite element analysis.

5.3. Finite element results

In Fig. 13 the results of Fig. 11, solid lines, are plotted together with the results from the finite element (FE) simulations, which include both the debond length and the crack tip position ($T_t = \hat{T}_t$ and V_{CNT}=10%). It should be noted that in these simulations no failure is taken into account for the UHMWPE fibre. The simulations run until extensive shear deformation in the polymer fibre close to the CTN end result in a non-convergent solution. It can be seen that the analytical model of Section 2.2, although a one-dimensional model, predicts quite accurately the stress for debonding initiation and captures the physics of debond growth. The difference in the slope of debond growth is mainly due to the Poisson's effect which is not included in the one-dimensional (shear-lag) analytical model and secondary to the anisotropic elastic properties used in the FE simulations. The predicted FE strengths for the different critical shear crack openings, are lower than the analytical predictions. The debond growth is in the order of 1 μm before excessive shear deformation in the polymer fibre occurs, compared to a debond growth in the order of millimeters for the analytical model. It should be noted that although the FE predicted debond length is significant, it is still approximately only 500 times the CNT radius. Clearly, the low shear properties of the highly anisotropic UHMWPE fibre limits the reinforcing efficiency of the CNTs. The predictions of the analytical model of Section 2.2 gives an upper bound for the strength of the CNT reinforced polymer fibres.

If the crack tip position is considered, then it can be seen that interface damage starts at an applied stress of around 0.2 GPa, i.e. an order of magnitude below the neat UHMWPE fibre strength and as expected independent of the critical opening, δ_t^f, which controls the length of the crack tip fracture process zone e.g. the higher the δ_t^f, the longer the fracture process zone and as a result delayed debonding initiation. The steady-state crack-tip fracture process zone can be calculated from the difference of x_{tip} and ℓ_d.

The effect of the interfacial frictional stress, based on FE simulations, is shown in Fig. 14 where again the analytical model predictions of Section 2.2 are included. Similar to Fig. 13, failure of the polymer fibre is not included in

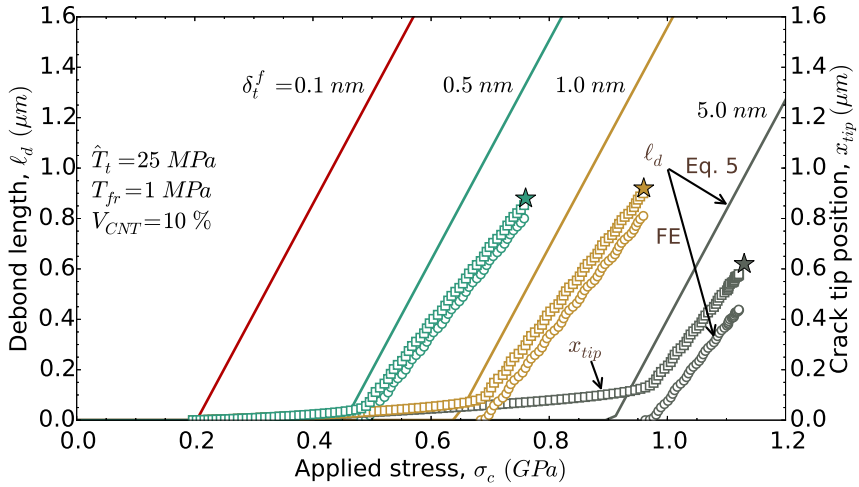

Figure 13: Finite element predictions of the crack tip position, x_{tip}, and debond length, ℓ_d, as a function of the applied stress, σ_c, for different critical interface shear crack openings, δ_t^f. The corresponding analytical predictions are based on the model of Section 2.2. AR =2000.

the FE model. The analytical model predictions are in fairly good agreement with the FE predictions. The differences observed are due to the mode II (shear) fracture energy, $\mathcal{G}_{c,t}^i$, being larger in the FE simulations for the same critical interfacial shear crack opening, δ_t^f. In the analytical model, $\mathcal{G}_{c,t}^i$ is calculated as the area under the traction-separation curve with T_t =0 for $\delta_t = \delta_t^f$. In the FE simulations $\mathcal{G}_{c,t}^i$ is the area under the traction-separation curve with $T_t = \hat{T}_{fr}$ for $\delta_t = \delta_t^f$ (see Fig. 3). However, the main conclusion from Fig. 14 is that a high interface frictional stress, results in higher shear deformation in the polymer fibre and the debond length is significantly lower compared to the analytical predictions. Thus, a high frictional stress, as indicated in Fig. 12, cannot be utilised to increase the CNT reinforced fibre strength.

Failure of the polymer matrix or fibre is included in the FE results of Fig. 15 where the crack tip position is plotted as a function of the applied stress for different shear failure strengths of the polymer fibre. The lowest shear strength value, 20 MPa, is lower than $\hat{T}_t$, and the largest value is four times higher than $\hat{T}_t$. The corresponding FE simulation, from Fig. 13, without shear failure of the polymer fibre is also included. As expected, the lower

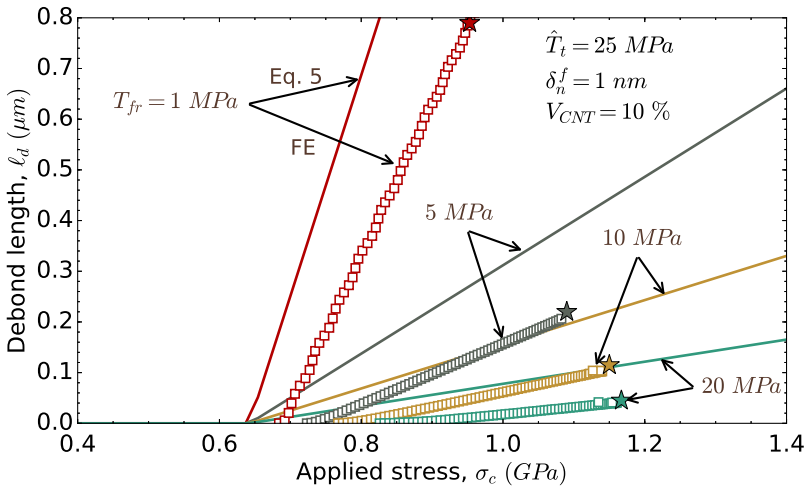

Figure 14: Finite element prediction of the debond length, ℓ_d, as a function of the applied stress, σ_c, for different interface frictional stresses, T_{fr}. The corresponding analytical predictions are based on the model of Section 2.2. AR =2000.

the shear strength of the polymer fibre, the lower the tensile strength of the CNT reinforced fibre and in all cases the predicted strength is significantly below that of simulations where failure of these highly anisotropic fibres is not considered. For σ_{12}^u equal to 20 MPa i.e. below $\hat{T}_t$, the reinforced fibre strength is nearly equal to the applied stress necessary to initiate damage near the interface. As σ_{12}^u increases, to 30 and 40 MPa, i.e. above $\hat{T}_t$, the interface fracture process zone develops but is not fully developed before failure of the fibre e.g. the debond length is zero (not shown in Fig. Fig. 15). For σ_{12}^u =50 MPa, i.e. twice $\hat{T}_t$, the debond length is only 0.25 nm when failure occurs. For fibre shear strengths much larger than $\hat{T}_t$, shear failure of these anisotropic polymer fibres is delayed and thus debonding initiates and grows prior to failure. For σ_{12}^u =100 MPa, the debonding length is about 35 nm ($\sim$24 r_{CNT}). Thus, increasing the interfacial peak traction, or in a less accurate term the interface strength, does not lead to a reinforcement of the polymer fibre because the limiting factor is the shear strength of the highly anisotropic polymer fibre itself, which is typically fairly low (20-80 MPa) for high performance polymer fibres like UHMWPE, PBO or PPTA.

Interestingly, from this work it can be concluded that the same property that limits the shear strength of macroscopic UHMWPE/epoxy or aramid/epoxy

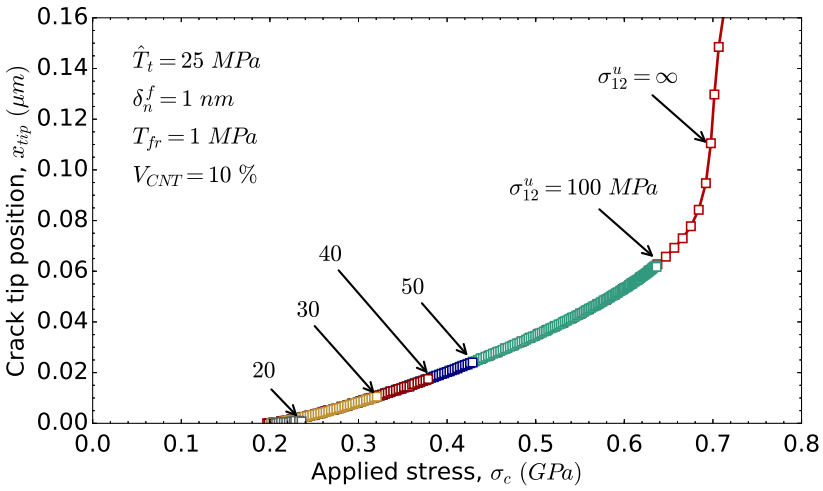

Figure 15: Finite element prediction of the crack tip position, x_{tip}, as a function of the applied stress, σ_c, for different shear failure strength values, σ_{12}^u, of the polymer (UHMWPE) fibre. The arrows, except for $\sigma_{12}^u = \infty$, indicate the point of failure. AR =2000.

composites [89, 103–105], limits the reinforcing efficiency of CNT reinforced UHMWPE or aramid nanocomposite fibres. For both systems ultimate strength is limited by the relatively low shear strength of the anisotropic fibres rather than interfacial adhesion.

Following these arguments it can now also be better understood why the oriented CNT reinforced PVA system of Wang et al. [53] was able to achieve such a high reinforcing efficiency with a near theoretical stress contribution by the SWCNTs of 88 GPa. Firstly, this system exhibited only a moderate overall fibre strength (∼1.2 GPa), reducing the need for a high CNT content and high interfacial shear stress. PVA is also a polar polymer and expected to show good interfacial adhesion. However, more importantly, the polar PVA has also a higher secondary bond strength between the chains than apolar PE, leading to a less anisotropic fibre. For example, the shear modulus of oriented PVA is reported to be about twice that of UHMWPE [39, 106]. Both effects, the lower overall strength and less anisotropic character of oriented PVA, lead to a nanocomposite fibre system where the ultimate strength is less dominated by the intrinsic shear strength of the oriented polymer fibre.

Similarly the favourable results of Chae et al. [107] may also be seen in this light. Here the authors reported an up to 60% increase in tensile strength

of carbonized PAN fibres with 1 wt% CNTs and an effective CNT stress of 67 GPa. Although the authors ascribed the increase in fibre properties to some extend to changes in the carbonization process and graphitic structure as a result of the presence of CNTs, i.e. a matrix effect rather than a direct nanotube reinforcement effect, the high reinforcing efficiency was here probably also aided by the higher shear properties of carbon fibre. Carbon fibres have a less anisotropic structure than UHMWPE or PPTA fibres. Graphite possesses strong covalent bonds between hexagonally arranged carbon atoms within the 2D layer-planes, but much weaker bonding between them [108]. Consequently carbon or graphite fibres can be considered as 2D structures as opposed to oriented polymer fibres like UHMWPE and PPTA, which can be considered as 1D structures as here covalent bonding only exists in the chain direction. Because of their less anisotropic character, carbon fibres have significantly higher shear properties. For example, the shear modulus of PAN based carbon fibre is around 14 GPa as compared to 0.8 and 2 GPa for UHMWPE and PPTA [39]. Again this will benefit a nanocomposite fibre system as the ultimate strength is less dominated by the poor shear properties of the fibre.

6. Conclusions

Analytical micromechanical models and finite element simulations were employed to explain why it is in practice so difficult to significantly reinforce high performance polymer fibres with CNTs. The main reason for the low reinforcing efficiency of CNTs in high performance polymer fibres are:

- The minimum CNT content required for effective reinforcement is relatively high and is in most cases well above than 5% and increases with polymer fibre modulus. Since it has been proven difficult to homogeneously disperse individual SWCNTs in polymers at high concentrations this will remain a challenge.

- A high interfacial shear strength or peak traction is required to prevent debonding of CNTs in the polymer fibre, however, such an increase in interface strength does not necessarily result in a higher fibre strength as often the limiting factor is the intrinsic shear strength properties of the highly anisotropic polymer fibre itself.

- Similarly, a positive contribution from an increase in interface fracture energy or critical crack opening is limited due to the highly anisotropy nature of most high performance polymer fibres.

- A high, albeit often unrealistic, interfacial frictional stress can increase the strength of the CNT reinforced polymer fibre, however only for (hypothetical) polymer fibres with high shear failure strength that exceeds the interfacial frictional stress.

- A high aspect ratio (>10000) of the CNTs has a significant positive effect on the polymer fibre strength as long as the polymer fibre does not fail by shear.

All factors listed above can in theory lead to CNT reinforced fibres with superior properties compared to commercial high performance polymer fibres if these highly anisotropic fibres were not inherently weak in directions other than the fibre direction. However, highly oriented polymer fibres are intrinsically anisotropic and possess low shear strengths. Therefore, it remains extremely doubtful if CNTs can significantly reinforce existing high performance polymer fibres like Kevlar®, Twaron®, Dyneema®, Spectra® or Zylon® with tensile strengths of around 3-5 GPa. Rather than mechanical reinforcement, here the creation of electrically conductive polymer fibres through nanotube modification [99, 109] or coatings [110] may be more promising. On the other hand, nanotube reinforcement might have some merit in textile grade fibres of lower mechanical performance such as nylon, polyester, polyacrylonitrile or poly(vinyl alcohol) or more isotropic carbon fibres.

Disclosure statement

No potential conflict of interest was reported by the authors.

Notes on contributors

Stergios Goutianos obtained his PhD from Queen Mary University of London in 2004 on the micromechanics of compressive failure in composites. He is currently a professor in the Department of Manufacturing and Civil Engineering at the Norwegian University of Science and Technology (NTNU),

having worked previously at the Technical University of Denmark and industry. His research expertise is in finite element modelling, mechanics, design and fracture mechanics of composites.

Ton Peijs is currently a professor in polymer engineering at WMG, University of Warwick (UK), having worked previously at Queen Mary University of London and Eindhoven University of Technology (Netherlands). His research is in the area of structure-processing-property relationships in polymer fibres, composites and nanocomposites. Other areas of research include multifunctional and sustainable polymeric materials.

References

[1] Thostenson ET, Ren Z, Chou TW (2001) Advances in the science and technology of carbon nanotubes and their composites: a review. Composites Science and Technology 61(13):1899–1912

[2] Spitalsky Z, Tasis D, Papagelis K, Galiotis C (2010) Carbon nanotube–polymer composites: Chemistry, processing, mechanical and electrical properties. Progress in Polymer Science 35(3):357–401

[3] Coleman J, Khan U, Gun'ko YK (2006) Mechanical reinforcement of polymers using carbon nanotubes. Advanced Materials 18(6):689–706

[4] Deng H, Barber AH, Peijs T (2010) Carbon nanotube/polymer composites. In: Sattler KD (ed) Handbook of nanophysics: functional nanomaterials, Topics in Applied Physics, GRS press, chap 1

[5] Iijima S (1991) Helical microtubules of graphitic carbon. Nature 354(6348):56–58

[6] Zhang H, Bilotti E, Peijs T (2015) The use of carbon nanotubes for damage sensing and structural health monitoring in laminated composites: a review. Nanocomposites 1(4):167–184

[7] Yakobson BI, Avouris P (2001) Mechanical properties of carbon nanotubes. In: Dresselhaus MS, Dresselhaus G, Avouris PH (eds) Carbon nanotubes: Synthesis, Structure, Properties and Applications, Topics in Applied Physics, vol 80, Springer-Verlag Berlin, Heidelberger Platz 3, D-14197 Berlin, Germany, pp 287–327

[8] Coleman JN, Khan U, Blau WJ, Gun'ko YK (2006) Small but strong: A review of the mechanical properties of carbon nanotube–polymer composites. Carbon 44(9):1624–1652

[9] Kinloch IA, Suhr J, Lou J, Young RJ, Ajayan PM (2018) Composites with carbon nanotubes and graphene: An outlook. Science 362:547–553

[10] Zhu HW, Xu CL, Wu DH, Wei BQ, Vajtai R, Ajayan PM (2002) Direct synthesis of long single-walled carbon nanotube strands. Science 296(5569):884–886

[11] Zhang M, Atkinson KR, Baughman RH (2004) Multifunctional carbon nanotube yarns by downsizing an ancient technology. Science 306(5700):1358–1361

[12] Ericson LM, Fan H, Peng H, Virginia VA, Zhou W, Sulpizio J, Wang Y, Booker R, Vavro J, Guthy C, Parra-Vasquez ANG, Kim MJ, Ramesh S, Saini RK, Kittrell C, Lavin G, Schmidt H, Adams WW, Billups WE, Pasquali M, Hwang WF, Hauge RH, Fischer JE, Smalley RE (2004) Macroscopic, neat, single-walled carbon nanotube fibers. Science 305(5689):1447–1450

[13] Koziol K, Vilatela J, Moisala A, Motta M, Cunniff P, Sennett M, Windle A (2007) High-performance carbon nanotube fiber. Science 318(5858):1892–1895

[14] Hayashi Y, Chiba Y, Inoue H, Hada M, Nishikawa T (2020) A review of dry spun carbon nanotube yarns and their potential applications in energy and mechanical devices. Journal of Fiber Science and Technology 76(2):72–78

[15] Wang W, Ciselli P, Kuznetsov E, Peijs T, Barber AH (2007) Effective reinforcement in carbon nanotube - polymer composites. Philosophical Transactions of the Royal Society A 366(1870):1613–1626

[16] Marom G, Wagner HD (2017) Should polymer nanocomposites be regarded as molecular composites? Journal Of Materials Science 52(8):8357–8361

[17] Vaisman L, Wagner HD, Marom G (2006) The role of surfactants in dispersion of carbon nanotubes. Advances in Colloid and Interface Science 128-130:37–46

[18] Ma P-C, Siddiqui NA, Marom G, Kim J-K (2010) Dispersion and functionalization of carbon nanotubes for polymer-based nanocomposites: A review. Composites Part A: Applied Science and Manufacturing 41(10):1345–1367

[19] Zalamea L, Kim H, Pipes RB (2007) Stress transfer in multi-walled carbon nanotubes. Composites Science and Technology 67(15):3425–3433

[20] Cui S, Kinloch IA, Young RJ, Noé L, M Monthioux M (2009) The effect of stress transfer within double-walled carbon nanotubes upon their ability to reinforce composites. Advanced Materials 21(35):3591–3595

[21] Ajayan PM (1995) Aligned carbon nanotubes in a thin polymer film. Advanced Materials 7(5):489–491

[22] Xie XL, Mai YW, Zhou XP (2005) Dispersion and alignment of carbon nanotubes in polymer matrix: A review. Materials Science and Engineering: R: Reports 49(4):89–112

[23] Martin CA, Sandler JKW, Windle AH, Schwarz MK, Bauhofer W, Schulte K, Shaffer MSP (2005) Electric field-induced aligned multi-wall carbon nanotube networks in epoxy composites. Polymer 46(3):877–886

[24] Kimura T, Ago H, Tobita M, Ohshima S, Kyotani M, Yumura M (2002) Polymer composites of carbon nanotubes aligned by a magnetic field. Advanced Materials 14(19):1380–1383

[25] Hobbie EK (2010) Shear rheology of carbon nanotube suspensions. Rheologica Acta 49(4):323–334

[26] Abbasi S, Carreau PJ, Derdouri A (2010) Flow induced orientation of multiwalled carbon nanotubes in polycarbonate nanocomposites: Rheology, conductivity and mechanical properties. Polymer 51(4):922–935

[27] Ciselli P, Wang Z, Peijs T (2007) Reinforcing potential of carbon nanotubes in oriented polymer fibres. Materials Technology 22(1):10–21

[28] Liu Y, Kumar S (2014) Polymer/carbon nanotube nano composite fibers–A review. ACS Applied Materials & Interfaces 6(9):6069–6087

[29] Mikhalchan A, Vilatela JJ (2019) A perspective on high-performance cnt fibres for structural composites. Carbon 150:191–215

[30] Deng L, Eichhorn SJ, Kao CC, Young RJ (2011) The effective young's modulus of carbon nanotubes in composites. ACS Applied Materials & Interfaces 3(2):433–440

[31] Zhang X, Shi X, Gautrot JE, Peijs T (2021) Nanoengineered electrospun fibers and their biomedical applications: A review. Nanocomposites 7(1):1–34

[32] Zhou W, Wu Y, Wei F, Luo G, Qian W (2005) Elastic deformation of multiwalled carbon nanotubes in electrospun MWCNTs–PEO and MWCNTs–PVA nanofibers. Polymer 46(26):12689–12695

[33] Sakurada I, Ito T, Nakamae K (1964) Elastic moduli of polymer crystals for the chain axial direction. Die Makromolekulare Chemie 75(1):1–10

[34] Nakamae K, Nishino T, Yokoyama F, Matsumoto T (1988) Temperature dependence of the elastic modulus of crystalline regions of poly(ethylene terephthalate). Journal of Macromolecular Science, Part B 27(4):407–420

[35] Yao J, Bastiaansen C, Peijs T (2014) High strength and high modulus electrospun nanofibers. Fibers 2(2):158–186

[36] Smith P, Lemstra P (1980) Ultra-high-strength polyethylene filaments by solution spinning/drawing. Journal of Materials Science 15:505–514

[37] Lemstra PJ, Kirschbaum R, Ohta T, Yasuda H (1987) High-strength/high-modulus structures based on flexible macromolecules: Gel-spinning and related processes. In: Ward IM (ed) Developments in Oriented Polymers—2, Springer, Dordrecht., chap 1, pp 39–49

[38] Lemstra PJ, Bastiaansen CWM, Peijs T, Jacobs MJ (2000) Fibres based on ultra-high molecular weight polyethylene: processing and applications. In: Ward IM, Coates PD, Dumoulin MM, Hyun KS (eds) Solid phase processing of polymers, Hanser Publishers, chap 1, pp 172–213

[39] Peijs T (2018) 1.5 high performance polyethylene fibers. In: Beaumont PWR, Zweben CH (eds) Comprehensive Composite Materials II, Elsevier, Oxford, pp 86–126

[40] Yang HH (1993) Kevlar aramid fiber. John Wiley & Sons, Chichester, UK

[41] Kearns JC, Shambaugh RL (2002) Polypropylene fibers reinforced with carbon nanotubes. Journal of Applied Polymer Science 86(8):2079–2084

[42] Jose MV, Dean D, Tyner J, Price G, Nyairo E (2007) Polypropylene/carbon nanotube nanocomposite fibers: Process–morphology–property relationships. Journal of Applied Polymer Science 103(6):3844–3850

[43] Deng H, Bilotti E, Zhang R, Peijs T (2010) Effective reinforcement of carbon nanotubes in polypropylene matrices. Journal of Applied Polymer Science 118(1):30–41

[44] Shen L, Gao X, Tong Y, Yeh A, Li R, Wu D (2008) Influence of different functionalized multiwall carbon nanotubes on the mechanical properties of poly(ethylene terephthalate) fibers. Journal of Applied Polymer Science 108(5):2865–2871

[45] Mun SJ, Jung YM, Kim JC, Chang JH (2008) Poly(ethylene terephthalate) nanocomposite fibers with functionalized multiwalled carbon nanotubes via in-situ polymerization. Journal of Applied Polymer Science 109(1):638–646

[46] Sandler JKW, Pegel S, Cadek M, Gojny F, van Es M, Lohmar J, Blau WJ, Schulte K, Windle AH, Shaffer MSP (2004) A comparative study of melt spun polyamide-12 fibres reinforced with carbon nanotubes and nanofibres. Polymer 45(6):2001–2015

[47] Gao J, Itkis ME, Yu A, Bekyarova E, Zhao B, Haddon RC (2005) Continuous spinning of a single-walled carbon nanotube - nylon composite fiber. Journal of the American Chemical Society 127(11):3847–3854

[48] Rangari VK, Yousuf M, Jeelani S, Pulikkathara MX, Khabashesku VN (2008) Alignment of carbon nanotubes and reinforcing effects in nylon-6 polymer composite fibers. Nanotechnology 18:19(24):245703

[49] Sreekumar T, Liu T, Min B, Guo H, Kumar S, Hauge R, Smalley R (2004) Polyacrylonitrile single-walled carbon nanotube composite fibers. Advanced Materials 16(1):58–61

[50] Chae HG, Sreekumar TV, Uchida T, Kumar S (2005) A comparison of reinforcement efficiency of various types of carbon nanotubes in polyacrylonitrile fiber. Polymer 46(24):10925–10935

[51] Zhang X, Liu T, Sreekumar VT, Kumar S, Hu X, Smith K (2004) Gel spinning of PVA/SWNT composite fiber. Polymer 45(26):8801–8807

[52] Xu X, Uddin AJ, Aoki K, Gotoh Y, Saito T, Yumura M (2010) Fabrication of high strength pva/swcnt composite fibers by gel spinning. Carbon 48(7):1977–1984

[53] Wang Z, Ciselli P, Peijs T (2007) The extraordinary reinforcing efficiency of single-walled carbon nanotubes in oriented poly(vinyl alcohol) tapes. Nanotechnology 18(45):455709

[54] Mai F, Deng H, Tu W, Chankajorn S, Fu Q, Bilotti E, Peijs T (2015) Oriented poly(lactic acid)/carbon nanotube composite tapes with high electrical conductivity and mechanical properties. Macromolecular Materials and Engineering 300(12):1257–1267

[55] Sandler J, Windle AH, Werner P, Altstädt V, Es MV, Shaffer MSP (2003) Carbon-nanofibre-reinforced poly(ether ether ketone) fibres. Journal of Materials Science 38(10):2135–2141

[56] Kumar S, Dang TD, Arnold EF, Bhattacharyya AR, Min BG, Zhang X, Vaia RA, Park C, Adams WW, Hauge RH, Smalley RE, Ramesh S, Willis PA (2002) Synthesis, structure, and properties of pbo/swnt composites&. Macromolecules 35(24):9039–9043

[57] Ruan SL, Gao P, Yang XG, Yu TX (2003) Toughening high performance ultrahigh molecular weight polyethylene using multiwalled carbon nanotubes. Polymer 44(19):5643–5654, in Honour of Ian Ward's 75th Birthday

[58] Ruan S, Gao P, Yu TX (2006) Ultra-strong gel-spun UHMWPE fibers reinforced using multiwalled carbon nanotubes. Polymer 47(5):1604–1611

[59] Wang Y, Cheng R, Liang L, Wang Y (2005) Study on the preparation and characterization of ultra-high molecular weight polyethylene–carbon nanotubes composite fiber. Composites Science and Technology 65(5):793–797

[60] Yeh JT, Lin SC, Chen KN, Huang KS (2008) Investigation of the ultradrawing properties of gel spun fibers of ultra-high molecular weight polyethylene/carbon nanotube blends. Journal of Applied Polymer Science 110(5):2538–2548

[61] Zhang S, Kumar S (2008) Carbon nanotubes as liquid crystals. Small 4(9):1270–1283

[62] Green MJ, Behabtu N, Pasquali M, Adams WW (2009) Nanotubes as polymers. Polymer 50(21):4979–4997

[63] Kumar S, Dang TD, Arnold FE, Bhattacharyya AR, Min BG, Zhang X, Vaia RA, Park C, Adams WW, Hauge RH, Smalley RE, Ramesh S, Willis PA (2002) Synthesis, structure, and properties of PBO/SWNT composites&. Macromolecules 35(24):9039–9043

[64] van Erp TB, Reynolds CT, Bilotti E, Peijs T (2019) Nanoclay assisted ultra-drawing of polypropylene tapes. Nanocomposites 5(4):114–123

[65] Van der Werff H, Marissen R (2006) Carbon nanotubes in high strength dyneema fibres. In: Proceedings of Polymer Fibres (on CDROM), Manchester, The International Polymer Fibre Conference,, pp 207–216

[66] Deng L, Young RJ, van der Zwaag S, Picken S (2010) Characterization of the adhesion of single-walled carbon nanotubes in poly(p-phenylene terephthalamide) composite fibres. Polymer 51(9):2033–2039

[67] Hale DK, Kelly A (1972) Strength of fibrous composite materials. Annual Review of Materials Science 2:405–462

[68] Sørensen BF (2017) Micromechanical model of the single fiber fragmentation test. Mechanics of Materials 104:38–48

[69] Belytschko T, Xiao SP, Schatz GC, Ruoff RS (2002) Atomistic simulations of nanotube fracture. Physical Review B 65:235430

[70] Dugdale DS (1960) Yielding of steel sheets containing slits. Journal of the Mechanics and Physics of Solids 8:100–104

[71] Barenblatt G (1962) The mathematical theory of equilibrium cracks in brittle fracture. Advances in Applied Mechanics 7:55–129

[72] Jiang LY, Huang Y, Jiang H, Ravichandran G, Gao H, Hwang KC, Liu B (2006) A cohesive law for carbon nanotube/polymer interfaces based on the Van der waals force. Journal of the Mechanics and Physics of Solids 54(11):2436–2452

[73] Jiang LY (2010) A cohesive law for carbon nanotube/polymer interface accounting for chemical covalent bonds. Mathematics and Mechanics of Solids 15(7):718–732

[74] Needleman A (1987) A Continuum Model for Void Nucleation by Inclusion Debonding. Journal of Applied Mechanics 54(3):525–531

[75] Camacho GT, Ortiz M (1996) Computational modelling of impact damage in brittle materials. International Journal of Solids and Structures 33(20):2899–2938

[76] Tvergaard V (1990) Analysis of tensile properties for a whisker - reinforced metal-matrix composite. Acta Metallurgica et Materialia 38:185–194

[77] Hashin Z, Rotem A (1973) A fatigue criterion for fiber-reinforced materials. Journal of Composite Materials 7:448–464

[78] Hashin Z (1980) Failure criteria for unidirectional fiber composites. Journal of Applied Mechanics 47:329–334

[79] Turon A, Dávila CG, Camanho PP, Costa J (2007) An engineering solution for mesh size effects in the simulation of delamination using cohesive zone models. Engineering Fracture Mechanics 74(10):1665–1682

[80] Sørensen BF, Goutianos S (2014) Mixed mode cohesive law with interface dilatation. Mechanics of Materials 70:76–93

[81] Goutianos S, Sørensen BF (2016) The application of J integral to measure cohesive laws under large-scale yielding. Engineering Fracture Mechanics 155:145–165

[82] Krishnan A, Dujardin E, Ebbesen TW, Yianilos PN, Treacy MMJ (1998) Young's modulus of single-walled nanotubes. Physical Review B 58:14013–14019

[83] E W Wong PES, Lieber CM (1997) Nanobeam mechanics: Elasticity, strength, and toughness of nanorods and nanotubes. Science 277:1971–1975

[84] Jin Y, Yuan FG (2003) Simulation of elastic properties of single-walled carbon nanotubes. Composites Science and Technology 63(11):1507–1515

[85] Giannopoulos GI, Kakavas PA, Anifantis NK (2008) Evaluation of the effective mechanical properties of single walled carbon nanotubes using a spring based finite element approach. Computational Materials Science 41(4):561–569

[86] Seidel GD, Lagoudas DC (2006) Micromechanical analysis of the effective elastic properties of carbon nanotube reinforced composites. Mechanics of Materials 38(8):884–907

[87] Gao XL, Li K (2002) A shear-lag model for carbon nanotube-reinforced polymer composites. International Journal of Solids and Structures 42:1649–1667

[88] Saether E, Frankland SJV, Pipes RB (2003) Transverse mechanical properties of single-walled carbon nanotube crystals. Part I: determination of elastic moduli. Composites Science and Technology 63(11):1543–1550

[89] Peijs T, Rijsdijk HA, de Kok JMM, Lemstra PJ (1994) The role of interface and fibre anisotropy in controlling the performance of polyethylene-fibre-reinforced composites. Composites Science and Technology 52(3):449–466

[90] Jhon YI, Kim C, Seo M, Cho WJ, Lee S, Jhon YM (2016) Tensile characterization of single-walled carbon nanotubes with helical structural defects. Scientific Reports 6:20324

[91] Mielke SL, Troya D, Zhang S, Li JL, Xiao S, Car R, Ruoff RS, Schatz GC, Belytschko T (2004) The role of vacancy defects and holes in the fracture of carbon nanotubes. Chemical Physics Letters 390(4):413–420

[92] Demczyk BG, Wang YM, Cumings J, Hetman M, Han W, Zettl A, Ritchie RO (2002) Direct mechanical measurement of the tensile strength and elastic modulus of multiwalled carbon nanotubes. Materials Science and Engineering: A 334(1):173–178

[93] Takakura A, Beppu K, Nishihara T, Fukui A, Kozeki T, Namazu T, Miyauchi Y, Itami K (2019) Strength of carbon nanotubes depends on their chemical structures. Nature Communications 10:3040

[94] Yu MF, Files BS, Arepalli S, Ruoff RS (2000) Tensile loading of ropes of single wall carbon nanotubes and their mechanical properties. Physical Review Letters 84:5552–5555

[95] Zu M, Li Q, Zhu Y, Dey M, Wang G, Lu W, Deitzel JM, Gillespie JW, Byun JH, Chou TW (2012) The effective interfacial shear strength of carbon nanotube fibers in an epoxy matrix characterized by a microdroplet test. Carbon 50(3):1271–1279

[96] Cooper CA, Cohen SR, Barber AH, Wagner HD (2002) Detachment of nanotubes from a polymer matrix. Applied Physics Letters 81:3873–3875

[97] Roy D, Bhattacharyya S, Rachamim A, Plati A, Saboungi ML (2010) Measurement of interfacial shear strength in single wall carbon nanotubes reinforced composite using raman spectroscopy. Journal of Applied Physics 107:043501

[98] Chen J, Yan L, Song W, Xu D (2018) Interfacial characteristics of carbon nanotube-polymer composites: A review. Composites Part A 114:149–169

[99] Ciselli P, Zhang R, Wang Z, Reynolds CT, Baxendale M, Peijs T (2009) Oriented UHMW-PE/CNT composite tapes by a solution casting-drawing process using mixed-solvents. European Polymer Journal 45(10):2741–2748

[100] Hull D, Clyne TW (2012) An Introduction to Composite Materials. Cambridge University Press, Cambridge, UK

[101] Şahin K, Clawson JK, Singletary J, Chasiotis I (2020) Shear strength of homopolymer and copolymer aramid fibers. Polymer 186:122034

[102] Young RJ, Liu M, Kinloch IA, Li S, Zhao X, Valles C, Papageorgiou DG (2018) The mechanics of reinforcement of polymers by graphene nanoplatelets. Composites Science and Technology 154:110–116

[103] Mercx FPM, Lemstra PJ (1990) Surface modification of aramid fibres. Polymer Communications 31(7):252–255

[104] Elkink F, Quaijtaal JHM (1989) Testing of fibre-matrix adhesion. In: Kleintjes LA, Lemstra PJ (eds) Integration of Fundamental Polymer Science and Technology, vol 3, Elsevier Applied Science, London, pp 228–234

[105] Wu SR, Sheu GS, Shyu SS (1996) Kevlar fiber–epoxy adhesion and its effect on composite mechanical and fracture properties by plasma and chemical treatment. Journal of applied polymer science 62(9):1347–1360

[106] Peijs T, van Vught RJM, Govaert LE (1995) Mechanical properties of poly(vinyl alcohol) fibres and composites. Composites 26(2):83–90

[107] Chae HG, Choi YH, Minus ML, Kumar S (2009) Carbon nanotube reinforced small diameter polyacrylonitrile based carbon fiber. Composites Science and Technology 69(3):406–413

[108] Blakslee OL, Proctor DG, Seldin EJ, Spence GB, Weng T (1970) Elastic constants of compression-annealed pyrolytic graphite. Journal of Applied Physics 41(8):3373–3382

[109] Bin Y, Chen Q, Tashiro K, Matsuo M (2008) Electrical and mechanical properties of iodine-doped highly elongated ultrahigh molecular weight polyethylene films filled with multiwalled carbon nanotubes. Physical Review B 77:035419

[110] Zhang R, Deng H, Valenca R, Jin J, Fu Q, Bilotti E, Peijs T (2012) Carbon nanotube polymer coatings for textile yarns with good strain sensing capability. Sensors and Actuators A: Physical 179:83–91

Graphical abstract

On the low reinforcing e ciency of carbon nanotubes in high performance polymer fibres

S. Goutianos , T. Peijs,